Ab Initio Adiabatic Dynamics Combined with Wigner Distribution Approach to Femtosecond Pump−Probe Negative Ion to Neutral to Positive Ion (NeNePo) Spectroscopy of Ag_2Au, Ag_4, and Au_4 Clusters

R. Mitrić,[†] M. Hartmann,[†] B. Stanca,[†] V. Bonačić-Koutecký,*[,†] and P. Fantucci[‡]

Walther-Nernst-Institut für Physikalische und Theoretische Chemie, Humboldt-Universität zu Berlin, Bunsenstrasse 1, D-10117 Berlin, Germany, and Dipartimento di Biotecnologie e Bioscienze, Università degli Studi di Milano, Bicocca Piazza della Scienza 2, I-20126 Milano, Italy

Received: May 8, 2001; In Final Form: June 28, 2001

Ultrafast ground state nuclear dynamics of small coinage metal clusters is theoretically explored in the framework of negative ion to neutral to positive ion (NeNePo) femtosecond pump−probe spectroscopy with the aim to determine the scope and perspective of this technique. This approach involves the preparation of an initial ensemble in the anionic ground state of the cluster, one-photon detachment by the pump pulse, the propagation of the system on the neutral electronic ground state, and detection via the cationic ground state by a time-delayed ionizing probe pulse. The calculations of the NeNePo-ZEKE signals under the condition of zero kinetic energy electrons are based on the combination of the Wigner distribution approach and ab initio molecular dynamics (MD) "on the fly" in the framework of gradient-corrected DFT for the propagation of an ensemble of classical trajectories and involves the average over the entire phase space. We have chosen examples of Ag_2Au and Au_4 to investigate time scales and the character of isomerization processes that are influenced by a local minimum corresponding to an energetically high-lying isomer with the structure related to the initial anionic structure. Capture of the nuclei within the local minimum takes place with dephased (Ag_2Au) or nondephased (Au_4) vibrational relaxation. Structural relaxations leading to isomerization processes are in both cases of delocalized nature and take place after 1 ps. In contrast, the Ag_4 cluster represents an example for which isomerization processes do not occur, since rhombic structures with slightly different bond lengths are global minima of the anionic and neutral ground states. Therefore, the relaxation dynamics is characterized by regular oscillations, which serve as fingerprints of structural properties. On the basis of the analysis of pump−probe signals and underlying dynamics, this contribution provides information about conditions under which structural properties of gas-phase clusters (global and local minima) and isomerization processes can be observed in the framework of the NeNePo-ZEKE type of spectroscopy. The latter is important in the context of applicability of this technique to the investigation of cluster reactivity.

I. Introduction

Increasing interest in ultrafast phenomena in chemistry, physics, and biology influenced development of new experimental femtosecond techniques[1,2] and theoretical approaches providing information on the nature of dynamical processes and determining conditions under which they can be observed.[3,4] Recent progress in experimental pump−probe femtosecond spectroscopy involves also application of the vertical one-photon detachment to prepare the nonequilibrium state of the metallic cluster and its subsequent investigation by two-photon ionization, which is known as NeNePo (negative ion to neutral to positive ion) technique pioneered by Wöste and his colleagues,[5−8] and extended by Lineberger et al.[9] using two-color excitation. Complementary to experiments, the development of a theoretical approach to multistate dynamics based on the combination of ab initio methods and Wigner−Moyal representation of the vibronic density matrix allowed us to determine the time scales and nature of different processes as well as conditions under which they can be observed in NeNePo[10,11] or other pump−probe or pump−dump experimental signals involving not only ground state but also excited electronic states.[12−15]

In our first theoretical study of the NeNePo femtosecond pump−probe signals of the $Ag_3^-/Ag_3/Ag_3^+$ cluster, three ground-state potential energy surfaces (PES) have been precomputed using ab initio quantum chemistry methods accounting for electronic correlation effects, and analytic expressions for pump−probe signals have been derived in the framework of the Wigner representation of the density matrix that require the calculation of an ensemble of classical molecular dynamics trajectories.[10,11] This approach allowed accurate simulations of pump−probe signals accounting for temperature-dependent initial conditions and for both zero electron kinetic energy (NeNePo-ZEKE) as well as considering the continuum states for the detached electron and the probed cation. The latter condition corresponds to the original NeNePo experimental situation.[5] The simulated NeNePo-ZEKE signals revealed in addition to the geometric relaxation (after electron detachment) from linear to triangular configuration a sudden internal energy redistribution from the bending to the stretching mode in the Jahn−Teller region of the triangular Ag_3 due to a strong repulsion of the terminal atoms. Time scales as well as the nature

* Corresponding author. Fax: +4930/2093 5573. Phone: +4930/2093 5576. E-mail: vbk@kirk.chemie.hu-berlin.de.
[†] Humboldt-Universität zu Berlin.
[‡] Università degli Studi di Milano.

10.1021/jp011759f CCC: $20.00
Published on Web 09/07/2001

of these processes are strongly influenced by the temperature of the initial ensemble. Moreover, the clear distinction between geometric relaxation and internal vibrational redistribution (IVR) in NeNePo-ZEKE signals is not any more present in simulated NeNePo signals that are in agreement with experimental findings. This reflected the fact that experimental conditions did not allow us to separate the two processes corresponding to geometric relaxation and to IVR. These findings stimulated new experiments in which the initial temperatures have been varied and consequently different time scales for geometric relaxation have been obtained in agreement with the theoretical predictions.[6,7] Moreover, additional experiments in the spirit of the NeNePo-ZEKE condition (reducing the excess of energy for the detached electron of the anion and of the cation) have been carried out.[6,8] To verify the conceptual framework of our semiclassical simulations based on Wigner distributions, a full quantum treatment of nuclei based on the same ab initio PES was performed.[16] The main features of NeNePo-ZEKE signals obtained from the Wigner distribution approach are in agreement with those obtained from the quantum dynamical treatment. The time scales of different processes are identical. Quantum dynamics modifies slightly relative signal intensities reflecting geometrical relaxation vs IVR due to delocalization of the wave packet.

Consequently, these studies gave us confidence to extend the Wigner distribution approach to larger systems in combination with ab initio molecular dynamics (MD) without precalculation of the energy surfaces. For this purpose the analytic gradients for the calculation of forces along the given electronic state are needed, which were not available. Therefore, we developed an ab initio adiabatic and nonadiabatic nuclear dynamics approach in electronic excited and ground states "on the fly" in the framework of a one-electron effective Hamiltonian, which is applicable to nonstoichiometric halide deficient clusters Na_nF_{n-1} characterized by strong ionic bonding and one excess electron.[14,15] Analytic formulation of gradients in excited states as well as of nonadiabatic couplings permitted calculations of trajectories at low computational demand. Consequently, the simulations of pump−probe and pump−dump signals have been carried out in the framework of the Wigner distribution approach combined with adiabatic and nonadiabatic MD "on the fly" involving also excited electronic states. This allowed us to determine time scales for breaking metallic and ionic bonds, geometric relaxation without bond breaking, different types of IVR,[14] and isomerization processes involving conical intersections.[15] To extend the applicability of MD "on the fly" for excited states of arbitrary systems, further theoretical developments are needed. In contrast, for the theoretical treatment of NeNePo signals the situation is simpler since in this case electronic ground states of negative ions, neutrals, and positive ions are involved, and therefore we use our MD "on the fly" based on the gradient-corrected density functional approach with Gaussian atomic basis (AIMD-GDF)[17] as a suitable tool in combination with the analytic formulation of NeNePo-ZEKE signals in the framework of the Wigner distribution approach.

In this contribution we present simulation and analysis of NeNePo-ZEKE signals for the mixed trimer of Ag_2Au and for both silver and gold tetramers. The choice of the systems have been made from three different points of view: (i) The study of dynamics of mixed trimer starting from the nonequilibrium state after one-electron detachment of linear Ag_2Au with peripheral position of the Au atom involves isomerization processes from one linear geometry with the peripheral position of the Au atom through triangular geometry to the linear isomer with the Au atom in the central position by forming the hetero Ag−Au bond and breaking the homo Ag−Ag bond. This offers an opportunity to study and to analyze dynamics of the heterotrimer exhibiting very different features with respect to those found for the $Ag_3^-/Ag_3/Ag_3^+$trimer. (ii) Structural properties of tetramers in the gas phase have not yet been experimentally accessible. Photodetachment data[18−22] and theoretical results[23] on Ag_4^- as well as optical response properties of Ag_4 and Ag_4^+ measured[24−27] and calculated[28] are available. From our previous work[23,29] it is known that in the case of the $Ag_4^-/Ag_4/Ag_4^+$ system the most stable structures of neutral and both charged tetramers are rhombic forms. Therefore, it is to be expected that the vibronic structure can be resolved in the NeNePo-ZEKE or related experiments, since the nonequilibrium state reached by one-photon detachment of the rhombic structure of Ag_4^- at low temperature of the initial ensemble is energetically close to the global rhombic minimum of the neutral Ag_4 (which is separated by the relatively large barrier from the second isomer with the T-form). Consequently, NeNePo-ZEKE technique can yield structural information via the vibronic structure, which can be theoretically identified in the simulated signals. Moreover, the experimental results in the spirit of NeNePo-ZEKE are available,[30] exhibiting vibrational structure. (iii) In contrast to the silver tetramers, anionic and neutral Au_4 clusters assume different geometries.[31,32] The energy ordering of isomers depends strongly on the details of the methods used. In the case of Au_4^-, linear and zigzag geometries are the lowest energy structures, while in the case of Au_4 the rhombic and the T-form are the most stable geometries. Therefore, simulation and analysis of the NeNePo signals should yield time scales and mechanisms of isomerization processes and at the same time provide stimulation for further experimental work.

The paper is structured in the following way: In section II the computational techniques are described. First, the accuracy of newly derived one-electron relativistic effective core potentials (1e-RECP) for the Au atom and a revised one for the Ag atom with corresponding AO basis sets will be addressed. Details of the derivation will be given in the Appendix. Second, the main features of ab initio MD based on gradient-corrected DF with Gaussian AO basis sets will be sketched, since the energy surfaces are not precalculated but the semiclassical trajectories are computed "on the fly". Third, the combination of ab initio MD and the Wigner distribution approach will be briefly described, allowing the simulation of pump−probe signals from analytic expressions that utilize the ensemble of semiclassical trajectories. In section III results and analysis of pump−probe NeNePo-ZEKE signals for mixed Ag_2Au trimers will be given. Sections IV and V contain our findings on silver and gold tetramers, respectively. Conclusions with outlook are presented in section VI.

II. Computational and Methodological

A. One-Electron Relativistic Effective Core Potentials (1e-RECP). In our previous work on structural and optical properties of silver clusters we developed 1- and 11-electron relativistic effective core potentials (1e-RECP[29]and 11e-RECP[28]), the first being suitable for the description of the ground-state properties and the second providing accurate results also for electronic excited states in connection with methods accounting for correlation effects. Since in this contribution calculations of an ensemble of trajectories are needed and therefore high accuracy and low computational demand is requested, we developed a new 1e-RECP for the Au atom and revised the one for the Ag atom with corresponding small AO basis sets based on the

TABLE 1: Atomic Data for Ag

(A) 1-Electron Relativistic Effective Core Potential

V_s			V_p		
n_{k0}	d_{k0}	ζ_{k0}	n_{kl}	d_{kl}	ζ_{kl}
0	4178.590964	6.497330	1	−0.117498	1.211027
0	−1.239270	0.044300	2	−0.024136	0.081884
1	−110.812405	128.580115			
1	2.918939	0.832404			
2	6.195014	2.573298			
2	−0.681654	1.999844			
2	−0.34342516	0.517329			

(B) Optimized Basis Set (6s/2p) with Contraction Scheme (3111/11)

a_k	c_k	a_k	c_k
1.48453761	0.167196	0.10000000	1
0.85850178	−0.388389	0.03500000	1
0.45500058	−0.079886		
0.08724483	1		
0.03462617	1		
0.00800000	1		

TABLE 2: Atomic Data for Au

(A) 1-Electron Relativistic Effective Core Potential

V_s			V_p		
n_{k0}	d_{k0}	ζ_{k0}	n_{kl}	d_{kl}	ζ_{kl}
0	4611.106671	8.607403	1	−36.609534	2.595141
0	−1.251252	0.007806	2	0.002547	0.087136
1	−258.202517	36.788884			
1	2.957278	0.833344			
2	6.201747	2.324319			
2	−0.673437	2.001872			
2	−0.343068	0.476917			

(B) Optimized Basis Set (7s2p) with Contraction Scheme (3211/11)

α_s	c_s	α_p	c_p
2.809000	−0.01277933	0.10000000	1
1.595000	−0.06415683	0.02000000	1
0.5327000	0.87562192		
0.282600	−0.84521682		
0.059800	−0.87412129		
0.020000	1		
0.010000	1		

gradient-corrected density functional calculations. New 1e-RECP's together with the AO basis sets for Ag and Au atoms are given in Tables 1 and 2, respectively. As described in the Appendix, they were derived by starting form our 11e-RECP for the Ag atom with original uncontracted 6s5p5d[28] basis and from 19e-RECP of Hay and Wadt[33] for the Au atom with their 8s6p4d uncontracted basis set using gradient-corrected density functionals of Becke[34] and Lee, Yang and Parr[35] (BLYP) for exchange and correlation, respectively. For this purpose atomic as well as diatomic data have been used in fitting procedures and therefore our 1e-RECP's are of the semiempirical type.

Comparison of the ground-state properties for atomic as well as homonuclear and heteronuclear neutral and charged dimers obtained with the 1e-RECP BLYP method with experimental values[19,36−39] are given in Table 3. The calculated bond distances are in satisfactory agreement with the measured values. The maximum deviations from experimental values for ionization potentials, electron affinities, and dissociation energies are ∼0.2 eV. The accuracy of calculated IP for Au_2 is difficult to judge since the experimental values have large error bars (cf. Table 3).

To verify the accuracy and the scope of our 1e-RECP in connection with the BLYP method for Ag_2 and Au_2 neutral and charged systems, we carried out calculations using the coupled cluster method with single and double excitations (CCSD). The values are almost identical with those obtained by BLYP calculations but in the case of adiabatic IP for Au_2, the CCSD method yields lower values (9.49 eV) than the BLYP approach (9.85 eV). We also examined the influence of different 19e-RECP's for Au introduced by Hay and Watt (HW),[33] Stevens et al. (SKB),[40] and Stuttgart RECP (S-RECP)[41,42] on the properties of gold dimers in the framework of BLYP and CCSD methods. All 19e-RECP's give rise to larger interatomic distances in comparison with experimental values. Notice that to obtain exact bond distances for Au_2, very elaborate relativistic calculations in the framework of the Douglas−Kroll transformation have to be carried out.[43] Values for IP and EA(VDE) obtained from BLYP and CCSD methods are comparable if very large basis sets with f-functions are used (cf. ref 44 and references therein).

Since a reliable determination of the energy ordering of different isomers is of particular importance, we extended the examination of the influence of different effective core potentials on neutral and charged gold tetramers in the framework of BLYP and CCSD approaches. Several common isomeric forms assuming linear (L), related zigzag structure (ZZ), rhombic (R), and T-form (with one atom attached to a triangle) are known,[31,32] with different energy orderings for Au_4^- than for Au_4 and Au_4^+. We payed particular attention to anions, since different statements concerning the applicability of density functional methods to atomic and molecular negative ions appeared in the litera-

TABLE 3: Ground States Properties for Dimers Obtained with the BLYP Method and 1e-RECP[a]

	symm	state	energy, au	d(A−B), Å	d(A−B), Å exp	IP_a, eV	IP, eV exp	EA_a, eV	VDE, eV	VDE, eV exp	D_e, eV	D_e, eV exp	ω_e, cm^{-1}	ω_e, cm^{-1} exp
Ag_2	$D_{\infty h}$	$^1\Sigma^+_g$	−0.62420	2.543	2.5303[b]	7.83	7.6557[b] (7.60)[d]	0.86	0.92	1.06[c]	1.83	1.65[c]	197	192.4[c]
AgAu	$C_{\infty v}$	$^1\Sigma^+$	−0.70590	2.493		8.85		1.20			2.00		198	
Au_2	$D_{\infty h}$	$^1\Sigma^+_g$	−0.77289	2.473	2.4719[c]	9.85	9.20[e]	1.66	2.12	2.01[c]	2.52	2.29[c]	180	190.9[c]
Ag_2^+	$D_{\infty h}$	$^1\Sigma^+_g$	−0.33632	2.776	*2.72*						1.57	1.65	124	*136*
$AgAu^+$	$C_{\infty v}$	$^1\Sigma^+$	−0.38052	2.706							1.10		123	
Au_2^+	$D_{\infty h}$	$^1\Sigma^+_g$	−0.41074	2.674	*2.74*						1.92	*2.57*	116	*170*
Ag_2^-	$D_{\infty h}$	$^1\Sigma^+_u$	−0.65581	2.684	2.600[c]						1.40	1.37	139	145[c]
$AgAu^-$	$C_{\infty v}$	$^1\Sigma^+$	−0.74986	2.632							1.30		138	
Au_2^-	$D_{\infty h}$	$^1\Sigma^+_u$	−0.83406	2.625	2.582[c]						1.92	1.92	123	149[c]

[a] Atomic energies are $E_{Au} = -0.340\,041$, $E_{Ag} = -0.278\,51$, $E_{Au^-} = -0.423\,46$, $E_{Ag^-} = -0.325\,85$, and $E_{Au^+} = E_{Ag^+} = 0.0$ au. Atomic values of IP and EA for both atoms are IP(Au) = 9.25(9.23), IP(Ag) = 7.58(7.58), EA(Au) = 2.27(2.31), and EA(Ag) = 1.23(1.30) eV; experimental values from ref 39 are in parentheses. For estimated values in italic compare Appendix. The core−core repulsion has been corrected according to $(CC(r_{ij}) = 1/r_{ij} + D\exp(-ar_{ij}))$. Constants D and a obtained for 1e-RECP's from the fitting procedure described in Appendix A necessery for corection of core−core potential: $D_{Ag-Ag} = 1619.887\,392$, $a_{AgAg} = 2.496\,301\,05$, $D_{Au-Au} = 1911.131\,090$, $a_{Au-A} = 2.465\,901\,29$, $D_{Au-Ag} = 1765.509\,532$, $a_{Au-Ag} = 2.481\,101\,17$. [b] Reference 36. [c] Reference 19. [d] Reference 37. [e] Reference 38.

ture.[45,46] The results can be summarized as follows: The energy ordering for Au_4^-, L < T < R, using 1e-RECP with BLYP and the CCSD method remains unchanged. All 19e-RECP's with the BLYP method favor slightly the zigzag (ZZ) form[31,32] closely related to the linear geometry, which became then a transition state.

The reason for this is that all 19e-RECP's yield too large distances for dimers in comparison with available experimental data. Since the zigzag (ZZ) form of Au_4^- has a shorter length than the linear (L) structure, all approaches yielding larger distances allow us to minimize the Coulomb repulsion of charges, due to an extra electron, which is localized at both ends already for the zigzag (ZZ) structure. Since our 1e-RECP is fitted to experimental data also for distances of dimers in the framework of the BLYP approach, it provides more realistic description of the bond lengths, which can be very important for determining relative energies of isomers.

In the case of the neutral Au_4 the energy ordering R < T < L remains also unchanged in BLYP and CCSD calculations with 1e-RECP. All three 19e-RECP's with BLYP approach stabilize the T-form so that it becomes degenerate with the rhombus (T $\approx$ R < L). Again, the accuracy of bond distances might play an important role. The situation is straightforward for Au_4^+ since all tested ECP's with BLYP give rise to the same energy ordering: R < T < L. In fact, all of them yield similar distances for Au_2^+ as the 1e-RECP. The CCSD calculations with 19e-RECP's require very large basis sets in order to yield reliable results.[44] The conclusion can be drawn that the most stable anionic structure of Au_4^- (linear or zigzag) differs from the neutral one (rhombic or T-form) independently of the details of the treatments. Quantitative accuracy of the individual approaches is difficult to judge. In conclusion, our newly developed 1e-RECP for Au with the corresponding AO basis set (Table 2) provides a practicable tool for the investigation of the general scope of NeNePo spectroscopy.

The situation for neutral and charged Ag clusters is expected to be simpler because d-electrons are strongly localized at Ag atoms and they do not contribute substantially to Ag−Ag bonding. Moreover, since the Ag−Ag distance is larger than the Au−Au distance, the Ag_4^- assumes the rhombic structure, since it is sufficiently large to allocate an extra electron, and both linear or zigzag structures lie energetically higher independently from the details of the treatments.

Therefore, the developed 1e-RECP with the corresponding basis set given in Table 1 is suitable for study of structural and dynamic ground-state properties of Ag clusters in the framework of the BLYP approach.

B. Ab Initio MD Approach "on the Fly". To study femtosecond dynamics of clusters as a function of their size, the precalculation of energy surfaces is not practicable, and therefore we employed our ab initio molecular dynamics code, which utilizes a Gaussian atomic basis set and gradient-corrected density functional (AIMD-GDF). The investigation of the dynamics of atoms is carried out by integration of the classical equations of motion using the Verlet algorithm. The SCF Kohn−Sham and the accurate calculation of forces are needed at each time step in order to achieve a satisfactory conservation of the total energy. All of this has to occur at low computational cost because the ensemble of trajectories is needed for the simulation of the pump−probe signals that utilize in addition to the ground-state trajectories of the neutral species, the energy gaps between neutral and cationic ground states. For small systems as those under consideration, the accurate numerical evaluation of the exchange-correlation energy parts of the Kohn−Sham matrix and the exchange-correlation energy derivatives are the most computationally demanding steps. Therefore, effort has been made to reach a good accuracy at relatively low cost (for the technical details cf. ref 17). The AIMD-GDF code has been used for calculations of trajectories for all three systems presented in this paper, Ag_2Au, Ag_4, and Au_4, although for the trimer the precalculation of the energy surfaces is feasible, as in the earlier work on Ag_3.

C. Wigner Distribution Approach. For the simulation of signals in the framework of NeNePo spectroscopy we have recently established the combination of the vibronic density matrix approach in classical Wigner−Moyal representation with ab initio molecular dynamics.[10,11] This approach involves the densities of the anionic state forming the initial ensemble, of the neutral state reached after photodetachment by the pump, and of the cationic state after photoionization by the probe, as well as the corresponding laser-induced transition probabilities between the states. Densities and transition probabilities can be explicitly calculated by invoking the classical approximation to the Wigner−Moyal transformed Liouville equation for the vibronic density matrix by restriction to the lowest order in $\hbar$. Furthermore, only the first-order optical transition processes are taken into account, which is justified for low laser intensities, and zero kinetic energy conditions (ZEKE) for the photodetached electron and the cation have been considered. Assuming Gaussian pulse envelopes with short laser pulse duration, an analytical expression for time-resolved NeNePo-ZEKE signals, which is given by the total occupation of the cationic state can be derived:[10]

$$S[t_d] \sim \int d\mathbf{q}_0\, d\mathbf{p}_0 \int_0^\infty d\tau_1 \exp\left\{-\frac{(\tau_1 - t_d)^2}{\sigma_{pu}^2 + \sigma_{pr}^2}\right\} \times \exp\left\{-\frac{\sigma_{pr}^2}{\hbar^2}[E_{pr} - V_{IP}(\mathbf{q}_1(\tau_1;\mathbf{q}_0,\mathbf{p}_0))]^2\right\} \times \exp\left\{-\frac{\sigma_{pr}^2}{\hbar^2}[E_{pu} - V_{VDE}(\mathbf{q}_0)]^2\right\} P_0(\mathbf{q}_0,\mathbf{p}_0) \quad (1)$$

In this expression, E_{pr} (E_{pu}) and σ_{pr} (σ_{pu}) are the excitation energies and pulse durations of the probe (pump) pulse, t_d is the time delay between pulses, and $V_{IP}(\mathbf{q}_1(\tau_1;\mathbf{q}_0,\mathbf{p}_0))$ denotes the time dependent energy gaps between cationic and the neutral electronic ground states calculated at coordinates $\mathbf{q}_1(\tau_1)$ on the neutral electronic ground state with initial coordinates and momenta $\mathbf{q}_0$ and $\mathbf{p}_0$ given by the anionic thermal Wigner distribution $P_0(\mathbf{q}_0,\mathbf{p}_0)$. Finally, $V_{VDE}(\mathbf{q}_0)$ are the vertical detachment energies of the initial anionic ensemble. This leads to the following steps needed for the simulations of the signals: (i) Generation of the initial anionic Wigner phase space distribution $P_0(\mathbf{q}_0,\mathbf{p}_0)$, which can be calculated either for single vibronic states or thermal ensembles invoking the harmonic approximation. In the present paper we assume a canonical initial ensemble for which the Wigner distribution of each normal mode is given by

$$P(q,p) = \frac{\alpha}{\pi\hbar} \exp\left[-\frac{2\alpha}{\hbar\omega}(p^2 + \omega^2 q^2)\right] \quad (2)$$

where ω is the normal-mode frequency and $\alpha = \tanh(\hbar\omega/2k_BT)$. This expression fully corresponds to the quantum mechanical density distribution and is suitable for low or moderate initial temperatures where anharmonic contributions of the nuclear motion can be neglected. In contrast, for higher temperatures

where quantum effects of the initial distribution are not important but anharmonicities are, the phase space distribution can be obtained from a long classical trajectory.[10] Sampling of the phase space distribution (2) yields the ensemble of initial conditions necessary for the molecular dynamics on the neutral state. The initial ensemble is photodetached and the Franck−Condon transition probability is given by the last exponential in expression (1). (ii) The ensemble is propagated on the neutral state using classical MD simulations "on the fly" providing the time dependent ionization energies V_{IP}. The probe step involves the transition to the cationic ground state with a window function determined by the second Exponential of expression (1). (iii) The final calculation of the signal involves the summation over the whole ensemble and the time resolution of the signal is determined by the pump−probe correlation function with the probe pulse window located around the time delay t_d between the pulses (first exponential of expression (1)).

Finally, we point out that quantum coherence effects are not taken into account in this approach, which is a consequence of the classical approximation. This is suitable for situations where the signals can be simulated by an ensemble of independent classical trajectories where all anharmonicities are included but quantum effects are not incorporated. In principle, the latter could be considered, e.g., by the initial value representation of Miller et al.,[47] which, however, would be difficult to observe directly in presently accessible NeNePo experiments.

III. Nuclear Dynamics and NeNePo-ZEKE Signals of Ag_2Au

The aim of the present investigation is to explore ultrafast relaxation processes of Ag_2Au on the neutral electronic ground state in the framework of NeNePo spectroscopy involving three isomers: a linear isomer with one homo- and one heterobond (Au−Ag−Ag), a triangular isomer, and another linear isomer with two heterobonds (Ag−Au−Ag) corresponding to the global minimum. We show that the simulated femtosecond NeNePo-ZEKE signals allow us to identify the isomers and to determine the time scales for the bond-breaking and bond-forming processes involved in the structural relaxation processes.

We start by discussing the structural properties of the anionic, the neutral, and the cationic ground states of Ag_2Au and by the presentation of the NeNePo pump−probe energy scheme. The anionic ground state of Ag_2Au^- is characterized by two linear isomers AI and AII with different locations of the Au atom (cf. Figure 1). Since the barrier of 0.22 eV is large, only the most stable isomer with the terminal Au atom contributes in the initial thermal ensemble involved in the NeNePo spectroscopy. Photodetachment of the asymmetric linear trimer (AI) generates a nonequilibrium state on the neutral ground state that is energetically close to the highest lying isomer III of the neutral trimer due to its geometrical similarity with the initial structure. The subsequent relaxation dynamics to the triangular isomer II and to the energetically close-lying most stable symmetric linear isomer I, involving the formation of a second heterobond and breaking of a homo Ag−Ag bond, respectively, can be monitored by the probe process with wavelengths between 6.13 eV (202 nm) and 7.69 eV (161 nm) (cf. Figure 1).

In our simulations, the initial anionic ensemble were obtained by sampling the canonical Wigner distribution (cf. section IIC). The normal-mode frequencies needed for the calculation of the Wigner distribution function are given in Table 4. The photodetachment process of the initial ensemble can be characterized by the histogram of vertical detachment energies (VDE) to the neutral ground state shown in Figure 2. It is centered around 2.78 eV, which corresponds to the VDE of the stable anionic linear geometry.

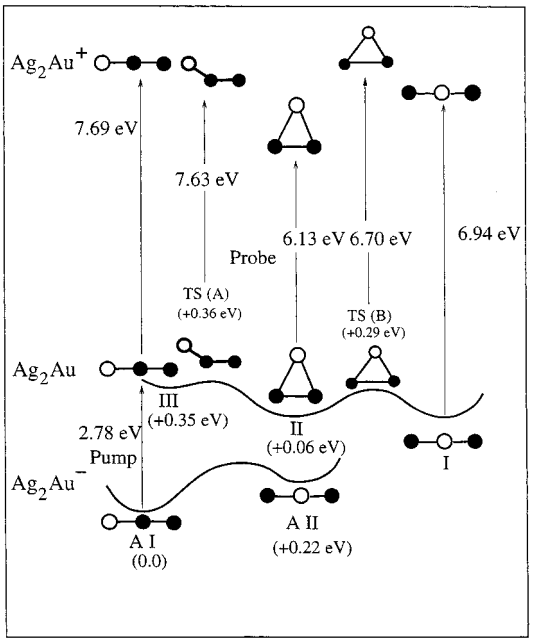

Figure 1. Scheme of the multistate femtosecond dynamics of Ag_2Au in the framework of the NeNePo pump−probe spectroscopy involving anionic (initial state), neutral (propagated state), and cationic (probe state) species (full and empty circles label Ag and Au atoms, respectively). Vertical transition energies are given by arrows. All corresponding geometries of isomers (AI, AII of the anion; I, II, III of the neutral) and transition states (TS(A) and TS(B)) are drawn. Numbers in parentheses are energies with respect to the ground electronic state of the corresponding most stable isomer.

As initial conditions for the MD simulations on the neutral electronic ground state we have chosen a set of 320 representative phase space points of the ensemble. The MD simulations have been performed "on the fly" up to a propagation time of 5 ps. We found that the dynamics is essentially characterized by two processes separated by different time scales: first, occupation of the linear isomer III (Au−Ag−Ag) after photodetachment and, second, isomerization toward the triangular structure. Both processes will be analyzed in the following.

The occupation of the asymmetric linear isomer III (Au−Ag−Ag, cf. Figure 1) can be visualized by the time evolution of the phase space density, which was represented by phase space points of the ensemble shown in Figure 3 up to 500 fs after photodetachment projected onto the (Ag−Ag distance)−(Ag−Au distance) potential energy surface (PES) (contour lines) for fixed linear geometry ($\alpha = 180°$). The latter were obtained by calculating the PES on a grid of 60 × 60 points for both distances for illustrative purposes. As can be seen from Figure 3, the nonequilibrium state reached after photodetachment ($t = 0$ fs) and represented by the phase space points is mainly characterized by a larger Ag−Au distance but a smaller Ag−Ag distance with respect to the asymmetric isomer III, which is located in the center of the contour lines. It can be easily seen (cf. structures above Figure 3) that the corresponding structural relaxation of the homo- and the heterobond, respectively, is comprised in the ω_3 mode (177 fs, cf. Table 4) superimposed by the ω_2 mode (322 fs), which, however, contributes only to the heterobond relaxation. The superposition of modes leading to a beating period of $2T_2T_3/(T_2 - T_3) = 786$ fs and a sum period of $2T_2T_3/(T_2 + T_3) = 220$ fs (with $T_2 = 322$ fs and $T_3 = 177$ fs, cf. Table 4), as well as anharmonicities,

TABLE 4: Energies, Geometries, Harmonic Frequencies, and Vibrational Periods for Isomeric Forms of Neutral and Charged Ag_2Au Clusters

	Ag_2Au^-		
isomer[a]	I($C_{\infty v}$)	II($D_{\infty h}$)	TS(C_{2v})
E (au)	−1.1094313	−1.101270	−1.066639
ΔE (eV)	0.0	0.22	1.16
r(Ag−Ag) (Å)	2.633		2.545
r(Ag−Au) (Å)	2.608	2.571	2.892
α (deg)	180.0	180.0	52.2
	ν/cm^{-1} (T/fs)		
ω_1	34.1 (977)[b]	33.2 (1000)[b]	−85.5
ω_2	103.9 (321)	130.6 (255)	72.9 (457)
ω_3	187.6 (178)	183.4 (181)	193.9 (172)
	Ag_2Au		
isomer[a]	I($D_{\infty h}$)	II(C_{2v})	III($C_{\infty v}$)
E (au)	−1.020727	−1.018625	−1.007889
ΔE (eV)	0.0	0.06	0.35
r(Ag−Ag) (Å)	2.561	2.581	2.671
r(Ag−Au) (Å)	2.561	2.680	2.546
α (deg)	180.0	57.5	180.0
	ν/cm^{-1} (T/fs)		
ω_1	19.1 (1744)[b]	55.8 (597))	9.0 (3687)[b]
ω_2	134.0 (249)	1.20.4 (277)	103.3 (322)
ω_3	179.2 (186)	188.5 (177)	186.6 (177)
	Ag_2Au^+		
isomer[a]	I(C_{2v})	II($D_{\infty h}$)	III($C_{\infty v}$)
E (au)	−0.793446	−0.766342	−0.725829
ΔE (eV)	0.0	0.74	1.84
r(Ag−Ag) (Å)	2.525	2.613	2.758
r(Ag−Au) (Å)	2.577	2.613	2.558
α (deg)	58.6	180.0	180.0
	ν/cm^{-1} (T/fs)		
ω_1	103.9 (321)	−21.3[b]	−29.2 b)
ω_2	148.2 (225)	122.3 (273)	89.1 (374)
ω_3	182.6 (182)	166.0 (201)	181.3 (184)

[a] Isomers (I, II, III) are labeled according to increasing energies; point group of the corresponding geometry is given in brackets. [b] Degenerate bending mode.

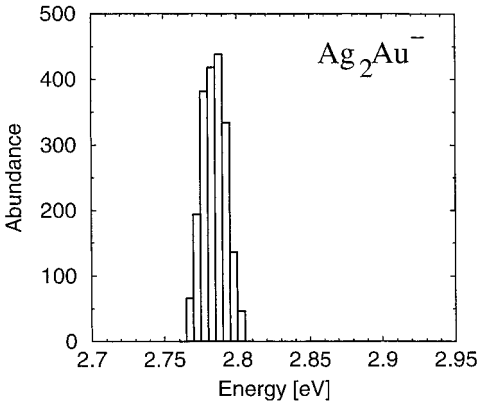

Figure 2. Histogram of the vertical detachment energies between the anion and neutral Ag_2Au for 50 K initial temperature ensemble obtained from 1000 phase space points.

lead to a rapid dephasing of the nuclear motion. The time scale of dephasing can also be determined from the time evolution of the phase space density (Figure 3). For very short times up to 200 fs after the Franck−Condon transition, dephasing has not yet remarkably influenced the dynamics, and therefore, one oscillation of the hetero- and homobond lengths (attributed to the center of mass motion of the ensemble) is observed. The period of ≈200 fs is on the order of the ω_3 (177 fs) mode. At 300 fs, dephasing of the dynamics leads to a separation of parts of the ensemble with strongly elongated Ag−Ag bond. After

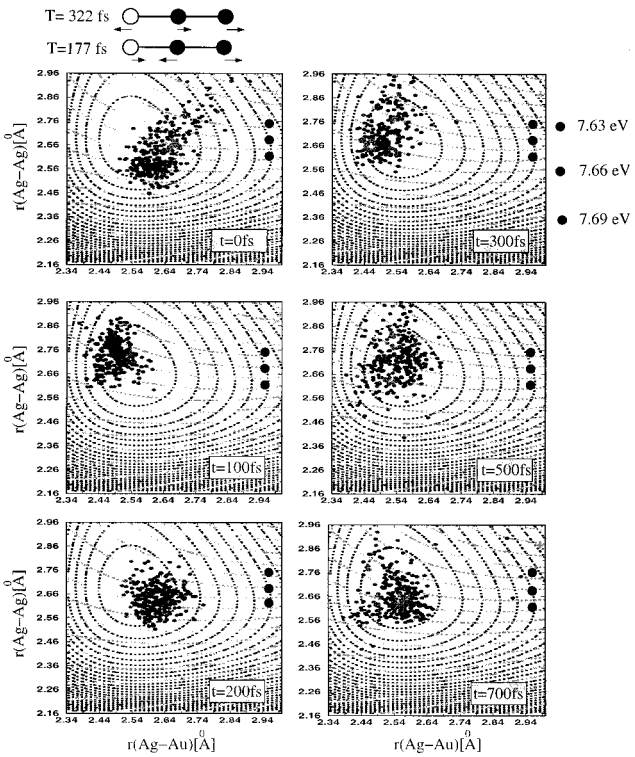

Figure 3. Snapshots of the time evolution of the phase space density (thick black dots) on the neutral ground state of Ag_2Au projected onto the two-dimensional cut of the potential energy surface along the Ag−Ag and Ag−Au distance and on the cation−neutral energy gap surface. The first is represented by round contours in the region of the linear asymmetric isomer (Au−Ag−Ag) at a fixed angle (α = 180°), and the latter is given by horizontal lines. Three representative energy gap values are indicated by large black cycles. Arrows in the geometry above refer to normal mode vibrations with frequencies ω_2 and ω_3 of the neutral Ag_2Au, respectively (cf. Table 4).

≈500 fs the ensemble occupies the whole local minimum. The beating period of 786 fs might cause the renewed localization of the phase space density at ≈700 fs. The features describes above are reflected in the signals which will be addressed below.

The bending mode of the system is separated from the stretching modes by an order of magnitude, as can be seen from the frequencies of Table 4. This low-frequency mode (≈9 cm^{-1}) leads to an isomerization. Its time scale can be determined by studying the projection of the phase space density on bending vs the Ag−Au distance shown in Figure 4. Obviously, isomerization to the triangular geometry starts at ≈900 fs. Moreover, this plot confirms the onset of dephasing at ≈300 fs.

Furthermore, we have studied the time dependent energy gaps between the cationic and the neutral ground states, which are essential quantities that determine the NeNePo signals (cf. section IIC). As can be seen in Figure 5, the bunches of energy gaps become localized at ≈200 fs corresponding to the nondephased dynamics of the ensemble during this time interval (cf. Figure 4). This quantity allows us also to identify the isomerization processes. At ≈900 fs, the energy gap values start to decrease, indicating the isomerization from the asymmetric linear III to the triangular isomer II, in agreement with the aforegiven analysis. As can be seen from Figure 5, the isomerization process is very irregular in time and spans an interval of several picoseconds. The main reason for this is again the particular shape of the local minimum, which is very flat along the bending coordinate (9 cm^{-1} (3687 fs), cf. Table 4); thus the time of isomerization depends sensitively on the initial bending coordinates and velocities given by the thermal

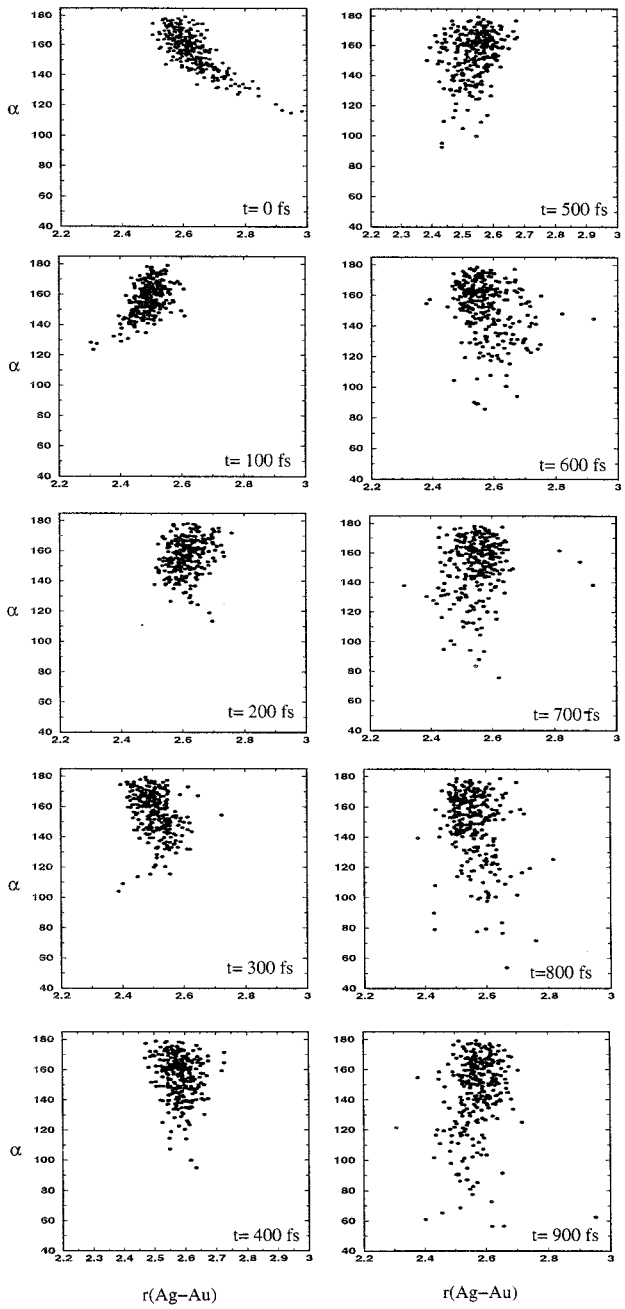

Figure 4. Snapshots of the time evolution of the phase space density on the neutral ground state of Ag_2Au projected onto the plane of bending and Ag−Au distance.

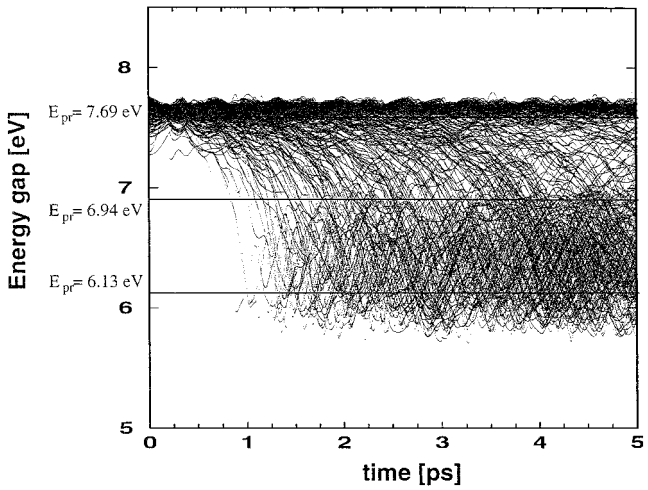

Figure 5. Bunch of energy gaps between the neutral and cationic state of Ag_2Au for 320 trajectories during the dynamics on the neutral electronic ground state obtained for initial temperature of 50 K. Energies given on the LHS refer to excitation energies of the probe pulse used for the simulation of the signals (cf. Figure 6).

ensemble. Isomerization of the triangular isomer II to the symmetric linear isomer I cannot be uniquely identified since the system gained a large amount of internal vibrational energy of more than 0.3 eV during structural relaxation. As a consequence, the phase space occupied by the system covers the basins of all three isomers. The spreading of the energy gaps in Figure 5 can be therefore attributed to continuous structural transformations of the system.

The MD calculations serve as input for the calculations of the NeNePo-ZEKE signals (cf. section IIC). Since we aim at the identification of the isomerization processes in the signals during the time evolution of the system, NeNePo-ZEKE signals were simulated at four different excitation energies (wavelengths) of the probe laser (cf. scheme Figure 1): 7.69 eV corresponding to the asymmetric linear isomer, 7.63 eV mainly probing the passage of the transition state to the triangular structure at a given time, 6.13 eV indicating the isomerization to the triangular isomer and finally 6.94 eV for the global minimum corresponding to the symmetric linear isomer. To be able to resolve the ultrafast structural relaxation, probe pulse durations of 100 fs were assumed. Concerning the photodetachment process, no selection of the initial phase space is considered. Therefore, zero pump pulse duration ($\sigma_{pu} = 0$) was assumed, allowing us to obtain comprehensive information on the ensemble dynamics on the neutral ground state.

The dynamics within the local minimum corresponding to the asymmetric isomer III is monitored by the 7.69 eV and the 7.63 eV signals shown in Figure 6a,b, respectively, up to 1 ps corresponding to the time scale before isomerization. The first peak of the 7.63 eV signal at 300 fs coincides with the minimum of the 7.69 eV signal (cf. Figure 6a,b), indicating the onset of dephasing in the dynamics of the system. This can be seen from the phase space occupation at 300 fs and its projection onto the cationic-neutral energy gap surface (gray dotted lines of Figure 3). Obviously, the separated part of the phase space crosses the 7.63 eV energy line. Furthermore, the peak of the 7.69 eV signal at 500 fs (cf. Figure 6a) corresponding to the minimum of the 7.63 eV signal can be attributed to the renewed localization of the phase space density due to constructive superposition of the ω_2 and ω_3 modes (cf. Figure 3 and energy lines). The beating period of $\approx$700 fs mentioned above is of course modified by anharmonicities.

Finally, the maximum of the 7.63 eV signal at 900 fs together with the minimum of the 7.69 eV signal as well as the onsets of the 6.13 and 6.94 eV signals indicate the beginning of isomerization toward the triangular structure in agreement with the analysis of the nuclear dynamics (cf. Figure 4 and discussion). The slowly rising intensities of the 6.13 and 6.94 eV signals indicate ongoing structural transformations involving the triangular as well as the global minimum corresponding to the symmetric linear isomer. However, the structureless shapes of the signals suggest strong thermal distortions. Thus, a particular isomer cannot be identified since the internal vibrational energy gained by the system after 1 ps is high due to the large excess of energy. As a consequence, the phase space density is spread, which is one of the reasons for the small intensities of both signals. On the other hand, only a smaller part of the phase space isomerizes within the time interval of 1−5 ps, as can be

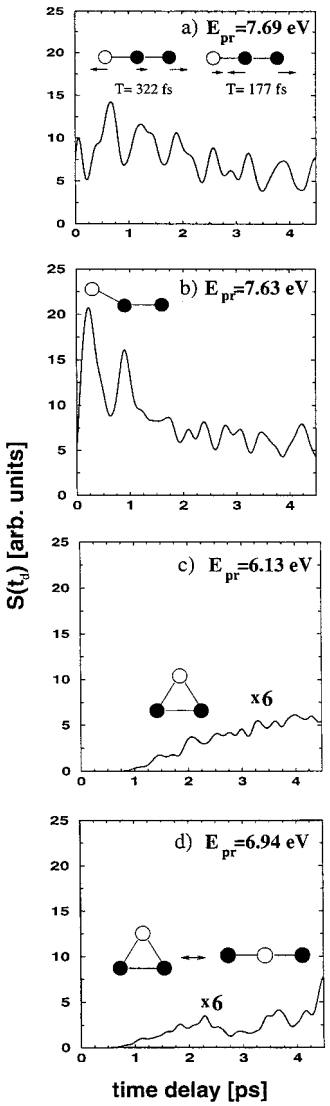

Figure 6. Simulated NeNePo-ZEKE pump−probe signals for 50 K initial ensemble of Ag_2Au at different energies of the probe pulse (a−d) corresponding to the geometries shown (cf. scheme Figure 1) and pulse duration of 100 fs. Signals in (c) and (d) were amplified by a factor of 6.

elucidated from the relatively large intensities and oscillating features of the 7.63 and 7.69 eV signals connected with the beating period described earlier, respectively. Therefore, we conclude that the local minimum with linear asymmetric structure captures the nuclei due to its particular shape characterized by two larger frequency stretching modes and a low-frequency bending mode. The stretching modes are superimposed by each other involving hetero- and homobond relaxation, which, however, does not superimpose with the bending mode, thus leading to a structural relaxation process that is widely spread in time over several picoseconds.

Finally, we point out that the character of the structural relaxation influenced by the local minimum is significantly different from the homonuclear $Ag_3^-/Ag_3/Ag^+$ system.[10,11] In the latter, a transition state is reached on the neutral ground state after photodetachment of the linear Ag_3^-, which leads to localized structural relaxation toward the triangular minimum geometry of the neutral Ag_3 on a time scale of less than 1 ps. As a consequence, the NeNePo-ZEKE signal shows only one strong peak corresponding to the structural relaxation when the system passes the probe window.

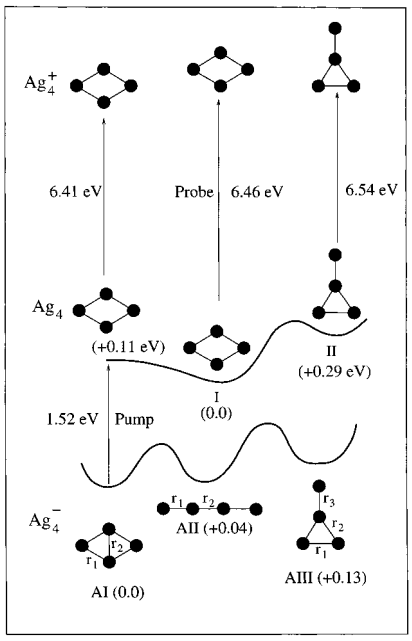

Figure 7. Scheme of the mulistate femtosecond dynamics of Ag_4 in the framework of the NeNePo pump−probe spectroscopy. Vertical transition energies are given by arrows. All corresponding geometries of isomers (AI, AII, AIII of the anion; I, II of the neutral) are drawn. Numbers in parentheses refer to energies with respect to the ground electronic state of the corresponding most stable isomer.

IV. Nuclear Dynamics and NeNePo-ZEKE Signals of Ag_4

In contrast to Ag_2Au, where the most stable isomers of the anion and neutral have different geometries, the most stable isomers of Ag_4^- and Ag_4 both assume rhombic geometry. This means that in the case of Ag_4^- the rhombic structure is sufficiently large to allocate an extra electron minimizing the Coulomb repulsion due to an additional electron. Therefore, both rhombic structures of Ag_4^- and Ag_4 are directly connected in the NeNePo process by excitation of normal modes without large amplitude motions. The aim of this section is to explore the characteristic features of the NeNePo signals in this case in connection with the underlying dynamics of normal modes and the structural signatures of the global minimum.

Figure 7 illustrates the NeNePo scheme, including energies and structures. Among the three isomers of the anionic ground state, the rhombic D_{2h} structure is the most stable one. The linear structure is almost degenerate but is well separated from the rhombic isomer by a large barrier. The third T-shape isomer is higher in energy by 0.12 eV and, therefore, a thermal distribution characterized only by rhombic geometry can be assumed for the initial ensemble in NeNePo spectroscopy at low temperatures. Photodetachment by the 1.52 eV pump pulse populates the neutral ground state where the relaxation toward the minimum can be monitored with probe pulse wavelengths between 6.41 and 6.46 eV. Isomerization to the second energetically high-lying T-shape isomer would require initial temperatures in the anionic state of more than 700 K. At this high initial temperature, however, isomerization in the anion would already occur, leading to a nonuniquely defined initial ensemble. Initial temperatures lower than ≈400 K, which prevent isomerization within the anionic state, have to be applied since the well-defined initial state is a necessary condition in NeNePo spectroscopy in order to be able to observe time scales and processes involved in the geometric relaxation of the neutral ground state.

TABLE 5: Energies, Geometries, Harmonic Frequencies, and Vibrational Periods for Isomeric Forms of Neutral and Charged Ag_4 Clusters

		Ag_4^-	
isomer[a]	I(D_{2h})	II($D_{\infty h}$)	III(C_{2v})
E (au)	−1.33641	−1.33491	−1.331869
ΔE (eV)	0.0	0.04	0.12
$r_1/r_2/r_3$ (Å)	2.716/2.773	2.648/2.702	2.734/2.749/2.628
		ν/cm^{-1} (T/fs)	
ω_1	34.5 (967)	15.2 (2191)[b]	22.3 (1494)
ω_2	80.5 (414)	37.8 (883)[b]	33.6 (991)
ω_3	92.8 (360)	79.4 (420)	87.3 (382)
ω_4	110.9 (301)	151.0 (221)	87.7 (380)
ω_5	148.4 (225)	182.4 (183)	131.5 (254)
ω_6	151.4 (220)		181.0 (184)

		Ag_4	
isomer[a]	I(D_{2h})	II(C_{2v})	III($D_{\infty h}$)
E (au)	−1.284787	−1.274036	−1.261466
ΔE (eV)	0.0	0.29	0.63
$r_1/r_2/r_3$ (Å])	2.723/2.569	2.555/2.817/2.572	2.570/2.766
		ν/cm^{-1} (T/fs)	
ω_1	36.4 (916)	1.0 (32511)	6.6 (5075)[b]
ω_2	80.7 (413)	24.8 (1343)	15.7 (2121)[b]
ω_3	90.2 (370)	77.7 (429)	72.3 (462)
ω_4	114.3 (292)	83.6 (399)	185.1 (180)
ω_5	165.1 (202)	188.3 (177)	197.6 (169)
ω_6	196.1 (170)	201.1 (166)	

	Ag_4^+	
isomer[a]	**I**(D_{2h})	II(C_{2v})
E (au)	−1.047743	−1.037783
ΔE (eV)	0.0	0.27
$r_1/r_2/r_3$ (Å)	2.716/2.773	2.633/2.708/2.748
	ν/cm^{-1} (T/fs)	
ω_1	18.0 (1852)	6.9 (4839)
ω_2	80.7 (413)	18.2 (1831)
ω_3	94.2 (354)	84.4 (395)
ω_4	101.3 (329)	116.3 (287)
ω_5	134.1 (249)	148.0 (225)
ω_6	178.9 (187)	182.1 (183)

[a] Isomers (I, II, III) are labeled according to increasing energies and point group of the corresponding geometry is given in brackets. [b] Degenerate bending mode.

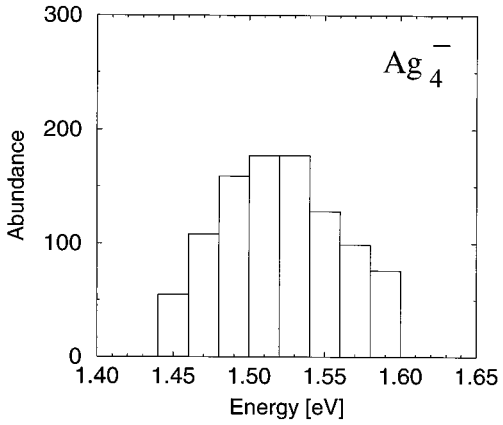

Figure 8. Histogram of the vertical detachment energies between the anion and neutral Ag_4 for 50 K initial temperature ensemble obtained from 1000 phase space points.

For the simulations we used an initial temperature of 50 K. The Wigner distribution of the corresponding canonical ensemble was calculated using the normal-mode frequencies of the rhombic anionic structure given in Table 5. The Franck−Condon profile shown in Figure 8 illustrates the photodetachment energies and possible wavelengths of the pump pulse. The maximum of the histogram at 1.52 eV corresponds to the vertical detachment energy of the anionic rhombic structure.

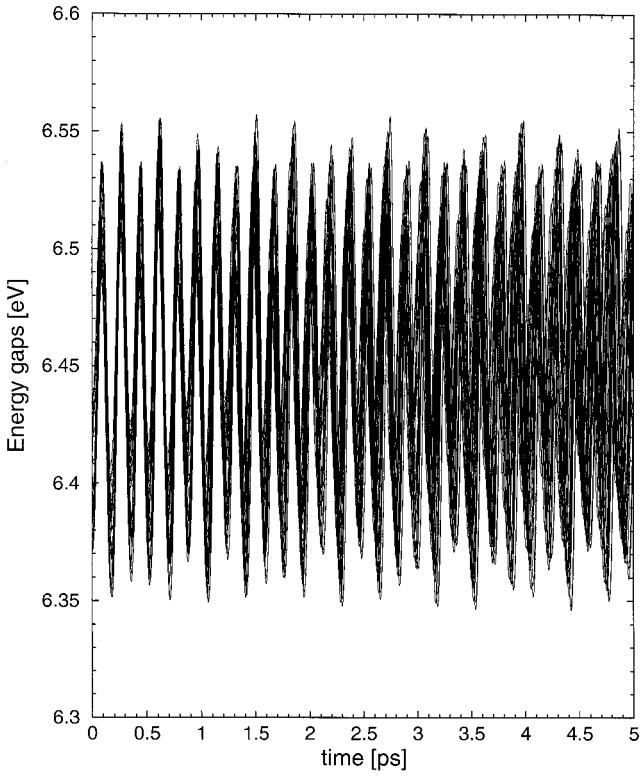

Figure 9. Bunch of the energy gaps between the neutral and cationic state of Ag_4 for 30 trajectories during the dynamics on the neutral electronic ground state obtained for initial temperature of 50 K.

MD simulations have been carried out on the neutral electronic ground state up to 5 ps starting from a set of 50 representative initial conditions of the ensemble. The relaxation of the rhombic structure toward the minimum of Ag_4 includes changes mainly in the short but also in the long diagonal, respectively, which are reflected in the ω_4 and ω_6 modes (cf. geometries given in Table 5). Therefore, the dynamics involves the excitation of these two modes with a larger contribution of the ω_4 mode. Other modes are weakly activated according to its occupation probability in the initial thermal ensemble. Only the lowest (ω_1) mode corresponding to a "butterfly" out-of-plane vibration contributes at the given low temperature of 50 K. The significant role of the particular modes for the femtosecond dynamics can be illustrated by studying the time dependent energy gaps between cationic and neutral ground electronic states, which also essentially determine the NeNePo signals. In Figure 9, a bunch of 30 energy gaps up to 5 ps are shown. As can be seen, they are strongly dominated by $T_6 =$ 170 fs (cf. Table 5), indicating the relaxation process along the short diagonal, as expected. Superposition with the other modes leads to increasing dephasing, which becomes visible after a propagation time of 2 ps.

On the basis of the MD simulations, NeNePo-ZEKE signals have been calculated at zero pump pulse duration ($\sigma_{pr} = 0$). Thus, the dynamics of the total initial phase space at a given temperature is considered, which is monitored at two different excitation wavelengths of the probe laser: $E_{pr} = 6.41$ eV (193.5 nm) corresponding to the initial rhombic configuration after photodetachment, and at $E_{pr} = 6.46$ eV (192 nm) offering information about the dynamics in the vicinity of the relaxed neutral rhombic structure corresponding to the global minimum (cf. scheme in Figure 7). The simulated NeNePo-ZEKE signal

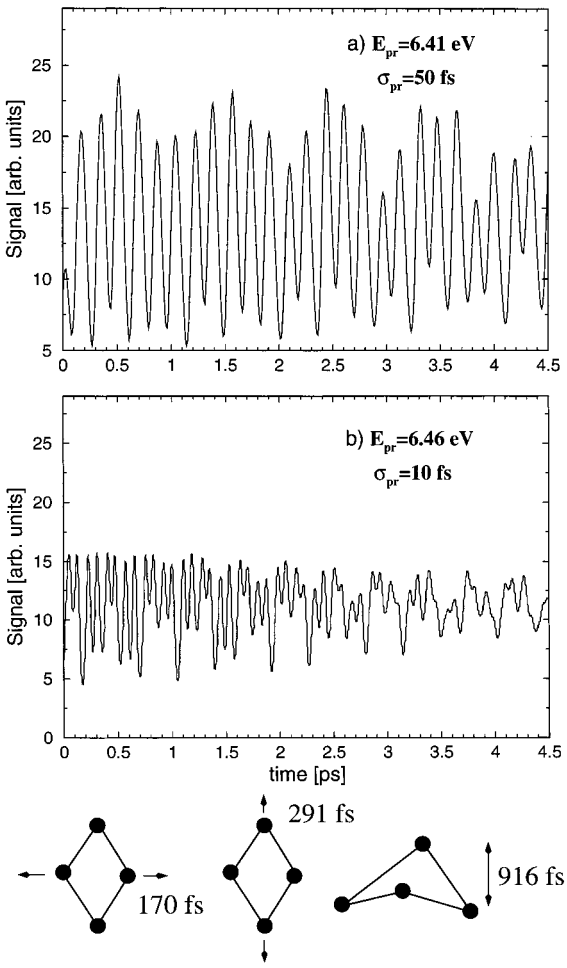

Figure 10. Simulated NeNePo-ZEKE pump−probe signals for 50 K initial ensemble of Ag_4 at different excitation energies E_{pr} and pulse durations σ_{pr} of the probe pulse. Normal modes contributing to the vibrational relaxation leading to signal oscillations are shown below.

at 6.41 eV for a probe pulse duration of 50 fs is shown in Figure 10a. The pronounced oscillations have a vibrational period of ≈175 fs, which is of the order of the ω_6 period (cf. Table 5), indicating the geometric relaxation along the short diagonal toward the global minimum. The Fourier analysis of the signal revealed modulation due to the ω_4 (long diagonal stretching) and the ω_1 ("butterfly") modes. Dephasing can be identified by studying the signal at $E_{pr} = 6.46$ eV . Since the probe window is passed twice by the energy gaps during one vibrational period, the probe pulse duration σ_{pr} has to be much shorter for an appropriate temporal resolution. In Figure 10b, the simulated NeNePo-ZEKE signal for $\sigma_{pr} = 10$ fs is shown. Up to 2 ps the signal is dominated by vibrations of 85 fs, which is half the period of the short diagonal vibration (ω_6 mode), as expected. However, after 2 ps the signal becomes apparently aperiodic, providing the time scale of dephasing of the system due to superposition with other modes.

Finally, we point out that the oscillatory features that are characteristic of the minimum rhombic structure could open the opportunity to identify a structure of a gas-phase cluster in experimental NeNePo signals.

V. Nuclear Dynamics and NeNePo-ZEKE Signals of Au_4

The stable isomers of Au_4^- and Au_4 are linear and rhombic, respectively, within our theoretical treatment. These different structural properties lead to large amplitude motions in the $Au_4^-/Au_4/Au_4^+$ NeNePo process. However, similar to Ag_2Au, the linear isomer is close to a high-lying isomer of the neutral Au_4. As a consequence, trapping effects in the local minimum influence the character and time scale of the isomerization dynamics. In this section we investigate the characteristic features of these processes in the NeNePo-ZEKE signals and compare the results with those obtained for Ag_2Au. Notice that the zigzag anionic form related to the linear structure obtained in other DFT treatments[31,32] would not change the main features of the processes involving the long amplitude motion under investigation.

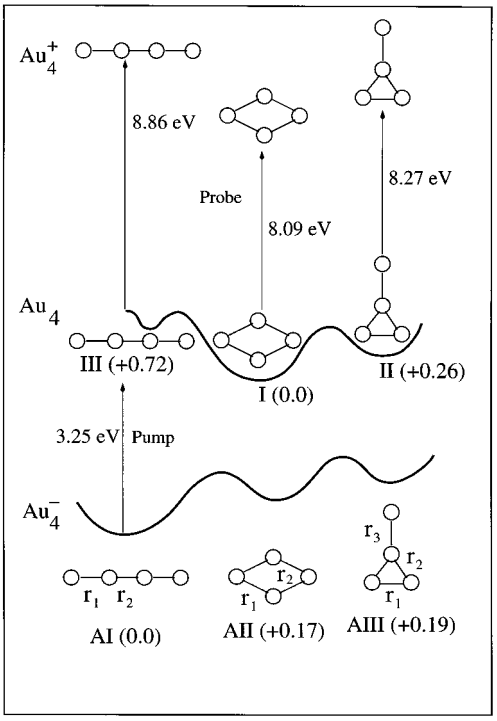

Figure 11. Scheme of the multistate femtosecond dynamics of Au_4 in the framework of the NeNePo pump−probe spectroscopy. Vertical transition energies are given by arrows. All corresponding geometries of isomers (AI, AII, AIII of the anion; I, II, III of the neutral) are drawn. Numbers in parentheses are energies with respect to the ground electronic state of the corresponding most stable isomer.

The NeNePo $Au_4^-/Au_4/Au_4^+$ scheme comprising energetic and structural information are shown in Figure 11. For the preparation of a uniquely defined initial ensemble, which is essential for NeNePo spectroscopy, low-temperature conditions have to be assumed in order to exclude thermal contributions of the higher lying rhombic and T-shape isomers. Then, only the linear isomer contributes to the initial ensemble, which is photodetached by an 3.25 eV (381 nm) pump pulse. The initiated relaxation dynamics on the neutral state involving linear, T-shape, and rhombic isomers can be monitored by two-photon ionization of the probe laser covering energy ranges (wavelengths) between 8.86 eV (140 nm) and 8.09 eV (153 nm).

In the simulations, the initial anionic ensemble has been obtained by sampling the canonical Wigner distribution by assuming a temperature of 50 K, and the corresponding normal-mode frequencies are given in Table 6. The histogram of vertical detachment energies providing information about the photodetachment process is shown in Figure 12. The maximum of the histogram reflects the VDE of the stable linear structure.

Starting from a set of 250 representative initial conditions of the ensemble, MD simulations on the neutral electronic ground state of Au_4 have been performed up to 5 ps. Since the initial nonequilibrium linear ensemble is close to the energetically

TABLE 6: Energies, Geometries, Harmonic Frequencies, and Vibrational Periods for Isomeric Forms of Neutral and Charged Au_4 Clusters

		Au_4^-	
isomer[a]	I($D_{\infty h}$)	II(D_{2h})	III(C_{2v})
E (au)	−1.684809	−1.678568	−1.677840
ΔE (eV)	0.0	0.17	0.19
$r_1/r_2/r_3$ (Å)	2.557/2.590	2.649/2.767	2.681/2.676/2.533
		ν/cm^{-1} (T/fs)	
ω_1	14.9 (2225)[b]	27.6 (1207)	18.3 (1821)
ω_2	31.8 (1049[b]	66.8 (499)	32.5 (1025)
ω_3	76.5 (436)	75.1 (444)	73.6 (453)
ω_4	141.0 (236)	91.9 (363)	78.1 (427)
ω_5	176.1 (189)	127.1 (262)	115.7 (288)
ω_6		129.4 (257)	167.7 (199)
		Au_4	
isomer[a]	I(D_{2h})	II(C_{2v})	III($D_{\infty h}$)
E (au)	−1.594328	−1.584677	−1.567974
ΔE (eV)	0.0	0.26	0.72
$r_1/r_2/r_3$ (Å)	2.637/2.527	2.492/2.744/2.438	2.491/2.722
		ν/cm^{-1} (T/fs)	
ω_1	29.6 (1128)	9.5 (3502)	8.6 (3602)[b]
ω_2	70.0 (476)	27.2 (1225)	19.0 (1751)[b]
ω_3	79.8 (418)	71.9 (463)	65.3 (510)
ω_4	102.8 (324)	73.9 (451)	171.8 (194)
ω_5	149.9 (222)	171.0 (195)	179.0 (186)
ω_6	171.3 (195)	184.4 (181)	
		Au_4^+	
isomer[a]	I(D_{2h})	II(C_{2v})	III($D_{\infty h}$)
E (au)	−1.298652	−1.286720	−1.240396
ΔE (eV)	0.0	0.32	1.58
$r_1/r_2/r_3$ (Å)	2.670/2.657	2.569/2.634/2.626	2.582/2.653
		ν/cm^{-1} (T/fs)	
ω_1	10.6 (3135)	5.2 (6376)	2.2 (14908)[b]
ω_2	72.4 (460)	23.1 (1445)	6.4 (5194)[b]
ω_3	84.7 (393)	80.3 (415)	70.2 (474))
ω_4	91.9 (363)	107.7 (309)	133.4 (250)
ω_5	125.2 (266)	136.4 (244)	180.6 (185)
ω_6	157.9 (211)	168.1 (198)	

[a] Isomers (I, II, III) are labeled according to increasing energies; point group of the corresponding geometry is given in brackets. [b] Degenerate bending mode.

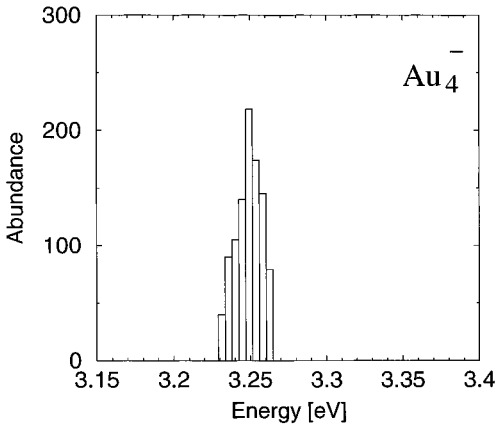

Figure 12. Histogram of the vertical detachment energies between the anion and neutral Au_4 for 50 K initial temperature ensemble obtained from 1000 phase space points.

highest linear Au_4 isomer, the relaxation dynamics is influenced by the structural properties of this isomer. Obviously, the geometric relaxation changing the bond lengths are contained in the ω_3, ω_4, and ω_5 normal modes, respectively (cf. bond lengths of the $D_{\infty h}$ isomers given in Table 6 and visualization of normal modes given in geometries of Figure 13). Each of the 2-fold degenerate bending modes ω_1 and ω_2 are only

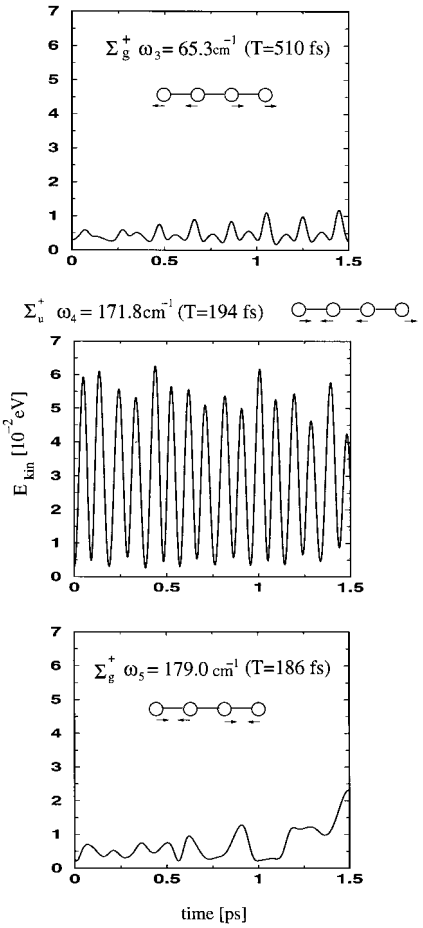

Figure 13. Ensemble-averaged kinetic energy decomposed into the ω_3, ω_4, ω_5 normal modes of the neutral linear structure (cf. Table 6) during the first 1.5 ps propagation on the neutral ground state of Ag_2Au.

thermally activated according to the occupation probability of the initial ensemble. Since the temperature is low, they practically do not influence the relaxation in the vicinity of the local minimum. To determine the contribution and significance of the particular modes in the relaxation process, the ensemble-averaged kinetic energies decomposed into the ω_3, ω_4, and ω_5 normal modes were investigated, as shown in Figure 13. It can be seen that the ω_4 mode is activated at most. This can be understood from the change of steepness between the potential surfaces of the anionic and neutral state along each normal mode, respectively, which can serve as characterization of the nonequilibrium state reached after photodetachment and estimated from the frequencies (cf. Table 6). For example, the ω_4 modes of the anion and the neutral are 141 and 171.8 cm^{-1}, respectively, and the curvatures are given by the square of these values. Thus, the steepness of the neutral state in the vicinity of the linear geometry is by ≈10 000 cm^{-2} larger along the ω_4 mode compared with the anionic state, leading to higher forces and consequently to strong activation of this mode.

Furthermore, we have studied the time dependent energy gaps between the cationic and the neutral ground states, which allow us to explore the isomerization processes from the linear toward the rhombic and T-shape structures. In Figure 14, bunches of all energy gaps are shown. Up to 1 ps, only regular oscillations are visible due to the strong activation of the ω_4 mode. In contrast to the dynamics of the Ag_2Au system, no dephasing by superposition with other modes is present on this time scale. Beyond 1 ps, onset of isomerization can be observed by

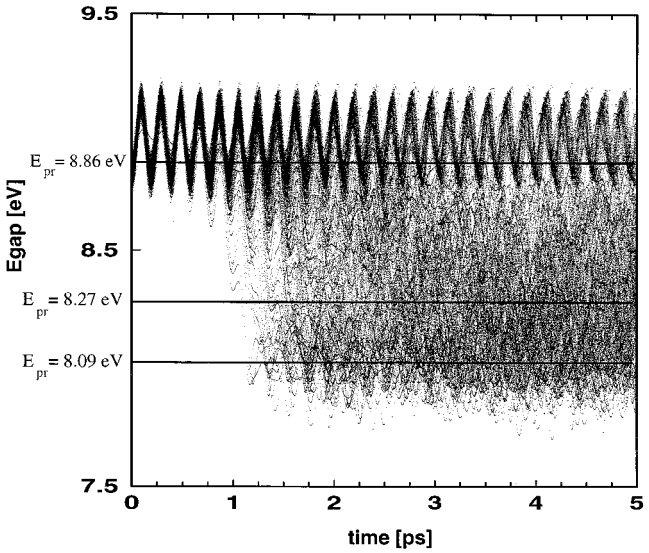

Figure 14. Bunch of the energy gaps between the neutral and cationic state of Au_4 for 250 trajectories during the dynamics on the neutral electronic ground state obtained for initial temperature of 50 K. Energies given on the LHS refer to excitation energies of the probe pulse used for the simulation of the signals (cf. Figure 15).

decreasing energy gap values. The isomerization process spans a long time interval and is not yet accomplished after 5 ps. This resembles to the Ag_2Au system: The flat potential surface along each of the bending modes characterized by the frequencies ω_1 and ω_2 (cf. Table 6), respectively, lead to sensitive dependence on the initial coordinates and momenta given by the thermal initial ensemble. Because of the high internal vibrational energy that the system gained after isomerization, the phase space covers a wide range of the potential surface and isomerization toward the T-shape isomer cannot be temporally identified.

On the basis of the MD simulations, calculations of NeNePo-ZEKE signals have been carried out. For the investigation of the ultrafast structural relaxation and isomerization, probe pulses of $\sigma_{pr} = 100$ fs at three excitation energies (wavelengths) has been assumed: $E_{pr} = 8.86$ eV corresponds to the initial Franck−Condon transition and allows us to identify the features of dynamics in the vicinity of the local linear isomer, whereas $E_{pr} = 8.09$ eV and $E_{pr} = 8.27$ eV are probing rhombic and T-shape isomers, respectively. To obtain comprehensive information about the dynamics, zero pump pulse duration ($\sigma_{pr} = 0$) was assumed for all calculations of signals. The signal at $E_{pr} = 8.86$ eV characterizing the dynamics within the local linear isomer reached immediately after the photodetachment is shown in Figure 15a. It is dominated by regular oscillations belonging to the ω_4 mode attributed to a nondephased relaxation process of the initial nonequilibrium ensemble (cf. Figure 13 and discussion). The signal intensity starts to decrease after 1 ps, indicating the linear to rhombic relaxation process. Consequently, the signal intensities at $E_{pr} = 8.09$ eV and $E_{pr} = 8.27$ eV increase (Figure 15b,c, where the 8.09 eV signal shows a weak maximum at $\approx$1.9 ps, indicating a temporally higher yield of the rhombic isomer. Otherwise, relatively structureless line shapes of both signals are a signature of the wide spread phase space occupation due to the large internal vibrational energy. Thus, particular isomerization involving rhombic or T-shape isomers cannot be identified as discussed above (cf. Figure 13 and discussion).

Finally, we emphasize that the absence of dephasing during the relaxation dynamics in the vicinity of the local linear isomer

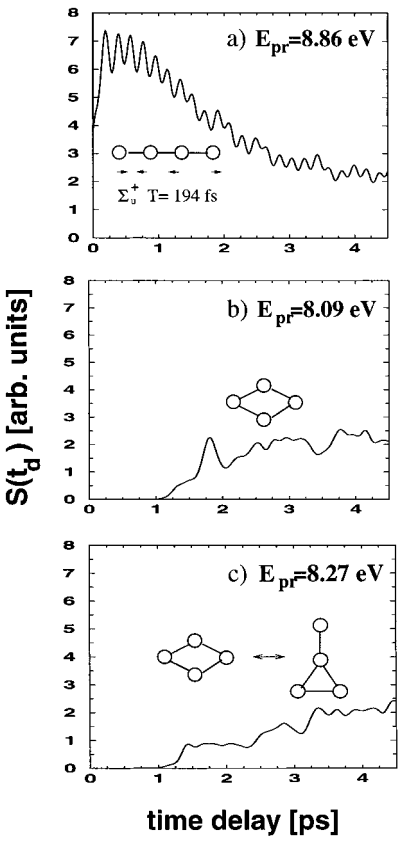

Figure 15. Simulated NeNePo-ZEKE pump−probe signals for 50 K initial ensemble of Au_4 at different excitation energies E_{pr} of the probe pulse (a−c) corresponding to the geometries shown (cf. scheme in Figure 11) and a pulse duration of 100 fs.

reveals the different character of the nonequilibrium state reached after photodetachment in comparison with the Ag_2Au system.

VI. Conclusions

We have theoretically investigated the ultrafast ground-state dynamics of Ag_2Au, Ag_4, and Au_4 clusters in the framework of the NeNePo-ZEKE pump−probe spectroscopy involving the anionic ground state for the preparation of an initial ensemble, the neutral ground state for the propagation of the system, and the cationic ground state for the probing. Our method is based on the Wigner distribution approach in combination with DFT BLYP classical trajectory simulations "on the fly", which allows an adequate treatment of optical excitation processes as well as ground-state nuclear dynamics. It is applicable for systems where quantum effects of the dynamics are washed out, e.g., due to the thermal motions of the nuclei. The results based on analysis of (A) dynamics and (B) simulated signals allow us to determine the scope of NeNePo spectroscopy as well as its perspectives. Now we summarize these aspects.

(A) First, our investigations revealed the connection between three objectives: The structural relation of anionic and neutral species, the nature of the nonequilibrium state reached after photodetachment by the pump pulse and the subsequent character of ultrafast neutral ground state dynamics. In general, the following situations can occur in which (i) the local minimum, (ii) the global minimum, and (iii) the transition state influences essentially the dynamics after photodetachment.

(i) In cases where the anionic structure (initial state) is close to a local minimum (energetically high-lying isomer) of the neutral electronic ground state (e.g., Ag_2Au, Au_4), the character

of the nonequilibrium state is governed by the local minimum. Vibrational relaxation within the local minimum is likely to dominate the ultrashort dynamics (on a time scale less than 1 ps for Ag_2Au and Au_4). Furthermore, in heteronuclear systems, strong dephasing due to superposition of particular modes and anharmonicities can occur due to simultaneously strongly activated modes, as found in the case of Ag_2Au. In contrast, homonuclear systems can exhibit nondephased regular vibrational relaxation. This has been found in the case of Au_4 where the pronounced activation of only one stretching mode takes place since the normal modes of the anionic and neutral species are almost identical.

Moreover, the local minimum can act as a strong capture area for nuclear motion with time scales up to several picoseconds. As a consequence, isomerization processes toward other and/or toward the global minimum structure are widely spread in time. In other words, structural relaxation dynamics is characterized as being incoherent and delocalized in phase space.

(ii) In cases where the anionic structure is close to the global minimum (stable isomer) of the neutral electronic ground state, vibrational relaxation reflecting the structural properties of the neutral stable isomer (e.g., Ag_4) takes place. The dynamics is dominated by one (e.g., Ag_4) or only a few modes given by the geometric deviations between anionic and neutral species. Other modes and anharmonicities weakly contribute, leading to dephasing on a time scale up to several picoseconds (longer than 2 ps for Ag_4).

(iii) In cases where the anionic structure is close to a transition state of the neutral electronic ground state (e.g., in the $Ag_3^-/Ag_3/Ag_3^+$ system) large amplitude motion toward the most stable isomer dominates the relaxation dynamics (on a time scale of $\approx$1 ps for the Ag_3 system). In other words, the dynamics is incoherent but localized in phase space. Different types of IVR can be initiated as consequence of the localized large amplitude motion.[10,11]

(B) Second, above-described different types of relaxation dynamics have been identified in simulated NeNePo-ZEKE signals, which means that they are in principle experimentally observable. These are again connected with the role of (i) the local minimum, (ii) the global minimum, and (iii) the transition state reached after photodetachment.

(i) Signals can exhibit (at different excitation wavelengths of the probe laser) fingerprints for dephased vibrational relaxation within the local minimum of heteronuclear systems (e.g., Ag_2Au), which takes place due to superposition of modes and perhaps anharmonicities. The time scale of the maxima and minima in signals can be attributed to the normal-mode frequencies of the local minimum. For homonuclear systems, regular oscillations of the signals serve as fingerprints of the nondephased vibrational relaxation as identified for Au_4 where the signal is dominated by one stretching mode.

After the systems escaped from the local minima the time scales for the beginning of the structural relaxation have been identified by the onset of signals at given probe wavelengths ($\approx$1 ps for Ag_2Au and Au_4), although the relatively structureless signals of low intensity reflect the delocalized character of the structural relaxation.

(ii) For the stable neutral isomer reached shortly after photodetachment, as in the case of Ag_4, vibrational relaxation gives rise to oscillations in NeNePo signals (for different pulse durations) that can be analyzed in terms of normal modes. Since the stable structure is characterized by the corresponding normal modes, this offers the opportunity to identify structural properties experimentally by the NeNePo technique.

(iii) In contrast to previous situations, large amplitude structural relaxation after the transition state is reached (as occurs in the case of Ag_3) gives rise to a pronounced single peak in NeNePo-ZEKE signals at a given time delay and probe excitation wavelengths. In addition, different types of subsequent IVR processes can be identified.[10,11]

In conclusion, characterization of the signals with respect to different dynamical processes including their time scales is of particular interest for proposing experimental conditions under which these processes can be revealed. In fact, the corresponding experimental work is in progress.[8,30]

Finally, we point out an important future aspect of the NeNePo technique. The desired occupation of a particular isomer can be induced by laser pulse shaping, and its reactivity with molecules can be examined in the probe step, thus allowing us to use NeNePo spectroscopy as a preparative tool to control the chemical reactivity of clusters and molecules.

Acknowledgment. This work was supported by the "Sonderforschungsbereich 450, Analyze und Steuerung photoinduzierter ultraschneller Reaktionen" of the *Deutsche Forschungsgemeinschaft*. The calculations have been partly carried out at the *Konrad-Zuse-Zentrum für Informationtechnik* Berlin.

VII. Appendix: Derivation of One-Electron Effective Core Potentials (1e-RECP)

The total potential is presented as

$$\hat{V}_l^{\mathrm{ECP}} = \sum_{l=0,1} \hat{V}_l^{\mathrm{ECP}}(r)[\sum_{m=-l}^{l} \hat{P}_{lm}] \tag{3}$$

where $\hat{P}_{lm}$ are angular projectors. The $\hat{V}_l^{\mathrm{ECP}}$ are analytically expressed in terms of products of Gaussians and powers of r as

$$r^2 V_l^{\mathrm{ECP}}(r) = \sum_k d_{kl} r^{n_{kl}} \mathrm{e}^{-\xi_{kl} r^2} \tag{4}$$

The quantities n_{kl}, d_{kl}, and ξ_{kl} can be considered as free fitting parameters. We outline shortly the optimization procedure for the s- and p-components of our 1e-RECP for silver and gold. It is expected that 1e-RECP reproduces the ionization energies and electron affinities of Ag and Au atoms in their neutral and negatively charged forms.

Therefore, to derive the s-component of 1e-RECP, we use as reference 5s valence orbitals for Ag and Ag^- obtained at the 11e-RECP BLYP level with corresponding fully uncontracted AO basis set 6s5p5d (cf. ref 28) and 6s valence orbitals for Au and Au^- computed at the 19e-RECP BLYP level with the 6s6p4d basis (cf. ref 33). The atomic energies are defined on the basis of experimental values:[39] $E(\mathrm{Ag}) = -\mathrm{IP} = -7.576$ eV $= -0.278\,427$ au; $E(\mathrm{Ag}^-) = -(\mathrm{IP} + \mathrm{EA}) = -8.878$ eV $= -0.326\,277$ au; $E(\mathrm{Au}) = -\mathrm{IP} = -9.23 = -0.339\,214$ au; $E(\mathrm{Au}^-) = -(\mathrm{IP} + \mathrm{EA}) = -11.54$ eV $= -0.424\,109$ au. In the case of the Ag atom 5s orbitals of the neutral and the anion form have been expanded in six s uncontracted orbitals and the matching between 11e- and 1e-RECP orbitals in the BLYP calculations has been carried out in the range between 0 and ∞, since the 11e-RECP 5s orbitals have no nodes in the core part. The best results obtained by fitting are $E(\mathrm{Ag}) = -0.278\,651$ au $= -\mathrm{IP} = 7.578$ eV and $E(\mathrm{Ag}^-) = -0.326\,36$ au giving rise to EA $= 1.298$ eV. The largest error is 0.004 eV. The form of s-component of 1e-RECP for Ag atom is given in Table 1.

Similarly, the matching between 1e and 19e pseudo-orbitals of Au atom has been carried out in the range from 1.533 to ∞, since the 5s and 6s orbitals of 19e-RECP cross at the radial values of 1.533 au. The best results from fitting procedure yield atomic energies $E(\mathrm{Au}) = -0.339\,84$ au and $E(\mathrm{Au}^-) = -0.424\,612$ au, which correspond to IP = 9.247 eV and EA = 2.307 eV, being in maximal error of 0.02 eV. The optimized s-part of 1e-RECP of Au atom is given in Table 2.

In summary, the s-components of the 1e-RECP have been derived by fitting the valence orbitals as functions of distances for neutral and negative atoms to the shape of valence orbitals from the 11e- or 19e-RECP's and to the experimental atomic data.

In molecular calculations, the s basis has been used in a contracted form and contraction coefficients are given in Tables 1 and 2. The atomic energies obtained with contracted AO basis sets in the BLYP calculation are used as reference values and are in good agreement with experimental values for IP and EA listed in Table 3.

Employing the optimized s-components, the optimization of the p-components for 1e-RECP has been carried out using available experimental data of neutral and charged dimers (distances, dissociation energies, harmonic vibrational frequencies, ionization potentials, and electron affinities) (cf. Table 3.). In the cases that experimental data are not available, the estimated values have been derived by scaling the theoretical results. For example, the ratio of the equilibrium distance for Ag_2 obtained with 11e-RECP BLYP and experimental value (2.568/2.53) gives a scaling factor 1.015, which is used to correct the equilibrium distance for Ag_2^+ obtained by 11e-RECP BLYP[28]calculation from 2.758 to 2.72 Å. All estimated values are labeled by italic numbers in Table 3. The optimized p-components of 1e-RECP together with the exponents of the AO basis sets are listed for Ag and Au in Tables 1 and 2, respectively.

Because of large size of the Ag and Au cores the point charge approximation for the core−core repulsion corresponding to the standard Coulomb potential must be corrected according to $CC(r_{ij}) = 1/r_{ij} + De^{-ar_{ij}}$ (cf. ref 29). Therefore, the repulsion curves for Me^+-Me^+ (Me = Ag, Au) have been calculated using our 11e-RECP for Ag_2^{2+} and 19e-RECP of Hay and Watt[33] for Au_2^{2+}. The constants D and a for which the fitting of the corresponding repulsion curves using 1e-RECP's have been calculated are listed in Table 3, and they introduce a sizable correction to the repulsion for distances relevant for bonding in Ag_n and Au_n clusters and are used throughout the paper. For the mixed Ag_2Au trimer, the averaged values between parameters obtained for Ag_2^{2+} and Au_2^{2+} have been employed (cf. Table 3).

References and Notes

(1) *Ultrafast Phenomena XII*; Elsaesser, T., Mukamel, S., Murname, M., Sherer N. F., Eds.; Springer: Berlin, 2000; Vol. 66.

(2) Zewail, A. *J. Chem. Phys. A* **2000**, *104*, 5660.

(3) Sundström, V., Ed. *Nobel Symposium Book: Femtochemistry and Femtobiology: Ultrafast Reaction Dynamics at Atomic-Scale Resolution*; World Scientific: Imperial College Press: London 1997.

(4) Mukamel, S. *Principles of Nonlinear Optical Spectroscopy*; Oxford University Press: Oxford, U.K., 1995.

(5) Wolf, S.; Sommerer, G.; Rutz, S.; Schreiber, E.; Leisner, T.; Wöste, L. *Phys. Rev. Lett.* **1995**, *74*, 4177.

(6) Wolf, S. Ph.D. Thesis, Department of Physics of the Freie Universität Berlin, Berlin 1997.

(7) Leisner, T.; Vajda, S.; Wolf, S.; Wöste, L.; Berry, R. S. *J. Chem. Phys.* **1999**, *111*, 1017.

(8) Hess, H.; Kwiat, S.; Socaciu, L.; Wolf, S.; Leisner, T.; Wöste, L. *Appl. Phys. B* **2000**, *71*, 337.

(9) Boo, D. W.; Ozaki, Y.; Anderson, L. H.; Lineberger, W. C. *J. Phys. Chem. A* **1997**, *101*, 6688.

(10) Hartmann, M.; Pittner, J.; Bonačić-Koutecký, V.; Heidenreich, A.; Jortner, J. *J. Chem. Phys.* **1998**, *108*, 3096.

(11) Hartmann, M.; Heidenreich, A.; Pittner, J.; Bonačić-Koutecký,V.; Jortner, J. *J. Phys. Chem. A* **1998**, *102*, 4069.

(12) Hartmann, M.; Pittner, J.; Dam, H.van; Bonačić-Koutecký, V. *Eur. Phys. J. D* **1999**, *9*, 393.

(13) Bonačić-Koutecký, V.; Hartmann, M.; Pittner, J.; van Dam, H. In *Cluster and Nanostructure Interfaces*; Jena, P., Khana, S. N., Rao, B. K., Eds.; World Scientific: Singapore, 2000; pp 1−8.

(14) Hartmann, M.; Pittner, J.; Bonačić-Koutecký,V. *J. Chem. Phys.* **2001**, *114*, 2106.

(15) Hartmann, M.; Pittner, J.; Bonačić-Koutecký, V. *J. Chem. Phys.* **2001**, *114*, 2123.

(16) Andrianov, I.; Bonačić-Koutecký,V.; Hartmann, M.; Manz, J.; Pittner, J.; Sundermann, K. *Chem. Phys. Lett.* **2000**, *318*, 256.

(17) Reichardt, D.; Bonačić-Koutecký, V.; Fantucci, P.; Jellinek, J. *Z. Phys. D* **1997**, *40*, 486.

(18) Ganteför, G.; Gausa, M.; Meiwes-Broer, K.-H.; Lutz, H. O. *J. Chem. Soc. Faraday Trans.* **1990**, *86*, 2483.

(19) Ho, J.; Ervin, K. M.; Lineberger, W. C. *J. Chem. Phys.* **1990**, *93*, 6987. Simard, B.; Hackett, P. A. *J. Mol. Spectrosc.* **1990**, *142*, 310. Ames, L. L.; Barrow, R. F. *Trans. Faraday Soc.* **1967**, *63*, 39.

(20) Handbusch, H.; Cha, C.-Y.; Möller, H.; Bechtold, P. S.; Ganteför, G.; Eberhardt, W. *Chem. Phys. Lett.* **1994**, *227*, 496.

(21) Handbusch, H.; Cha, C.-Y.; Bechtold, P. S.; Ganteför, G.; Eberhardt, W. *J. Chem. Phys.* **1995**, *102*, 6406.

(22) Taylor, K. J.; Pettiette-Hall, C. L.; Chesnovsky, O.; Smalley, R. E. *J. Chem. Phys.* **1992**, *96*, 3319.

(23) Bonačić-Koutecký, V.; Češpiva, L.; Fantucci, P.; Pittner, J.; Kouteck, J. *J. Chem. Phys.* **1994**, *98*, 490.

(24) Collings, B. A.; Athanassenas, K.; Lacombe, D. M.; Rayner, D. M.; Hackett, P. A. *J. Chem. Phys.* **1994**, *101*, 3506.

(25) Félix, C.; Sieber, C.; Harbich, W.; Buttet, J.; Rabin, I.; Schulze, W.; Ertl, G. *Chem. Phys. Lett.* **1999**, *313*, 105.

(26) Terasaki, A.; Minemoto, S.; Iseda, M.; Kondow, T. *Eur. Phys. J. D* **1999**, *9*, 163−168.

(27) Schloos, D.; Gilb, S.; Kaller, J.; Kappes, M. M.; Furche, F.; Köhn, A.; May, K.; Ahlrichs, R. *J. Chem. Phys* **2000**, *113*, 5361.

(28) Bonačić-Koutecký, V.; Pittner, J.; Boiron, M.; Fantucci, P. *J. Chem. Phys.* **1999**, *110*, 3876.

(29) Bonačić-Koutecký, V.; Češpiva, L.; Fantucci, P.; Pittner, J.; Koutecký, J. *J. Chem. Phys.* **1993**, *98*, 7981.

(30) Hess, H.; Asmis, K. R.; Leisner, T.; Wöste, L. *Eur. Phys. J.*, in press. Femtosekunden-Spektroskopie an kleinen Metallclustern. Ph.D. Thesis, Department of Physics of the Freie Universität Berlin, Berlin 1999.

(31) Häkkinen, H.; Landman, U. *Phys. Rev. B* **2000**, *62*, 2287.

(32) Grönbeck, H.; Andreoni, W. *Chem. Phys.* **2000**, *262*, 1.

(33) Hay, P. J.; Wadt, W. R. *J. Chem. Phys.* **1985**, **82**, 270. Wadt, W. R.; Hay, P. J. *J. Chem. Phys.* **1985**, *82*, 284. Hay, P. J.; Wadt, W. R. *J. Chem. Phys.* **1985**, *82*, 299.

(34) Becke, A. D. *Phys. Rev. A* **1988**, *98*, 3098.

(35) Lee, C.; Yang, W.; Parr, R. G. *Phys. Rev. B* **1988**, *37*, 785.

(36) Beutel, V.; Krämer, H. G.; Bhale, G. L.; Kuhn, M.; Weyers, K.; Demtröder, W. *J. Chem. Phys.* **1993**, *98*, 2699.

(37) Jackslath, C.; Rabin, I.; Schulze, W. *Z. Phys. D* **1992**,*22*, 517.

(38) Jackslath, C.; Rabin, I.; Schulze, W. *Ber. Bunsen-Ges. Phys. Chem.* **1992**, *96*, 1200.

(39) Moore, C. E. Atomic energy levels, Circ. No. 467; Nat. Bureau of Standards: Washington, DC, 1958; Vol. III.

(40) Stevens, W. J.; Krauss, M.; Basch, H.; Jasien, P. G. *Can. J. Chem.* **1992**, *70*, 612.

(41) Andrae, D.; Häussermann, U.; Dolg, M.; Stoll, H.; Preuss, H. *Theor. Chim. Acta* **1990**, *77*, 123.

(42) Martin J. M. L.; Sundermann, A. *J. Chem. Phys.* **2001**, *114*, 3408.

(43) Hess B. A.; Kaldor, U. *J. Chem. Phys.* **2000**, *112*, 1809.

(44) Wesendrup, R.; Hunt, T.; Schwerdtfeger, P. *J. Chem. Phys.* **2000**, *112*, 9356.

(45) Galbraith J. M.; Schaefer, H. F. *J. Chem. Phys.* **1996**, *105*, 862.

(46) Rösch, N.; Trickey, S. B. *J. Chem. Phys.* **1997**, *106*, 8940.

(47) Miller, W. H. *Faraday Discuss.* **1998**, *110*, 1.